npj | parkinson's disease

Article

Published in partnership with the Parkinson's Foundation

https://doi.org/10.1038/s41531-025-00994-1

Resilience of striatal synaptic plasticity over early structural adaptations in premotor parkinsonism

Leyre Merino-Galán[1,2,3], Marta Zamarbide[1], Arantzazu Belloso-Iguerategui[1,4], Marta C. Alonso-Moreno[1,5], Belén Gago[6], Alejandro Reinares-Sebastián[7,8,9,10], Javier Blesa[7,8,9,10], Dani Dumitriu[11], Ana Quiroga-Varela[1,12,15] & María Cruz Rodríguez-Oroz[1,13,14,15] ✉

Parkinson's disease has a long premotor phase with ongoing dopaminergic degeneration, yet its compensatory mechanisms remain unclear. Using a rat model with A53T α-synuclein overexpression in the substantia nigra, we analyzed striatal synaptic changes at 72 h, 1, 2, and 4 weeks post-inoculation, before motor signs appeared. Dopamine concentration decreased from 72 h, and chemical long-term potentiation was simultaneously inhibited, partially recovering by 4 weeks. At this time point, dopaminergic degeneration and post-synaptic morphological and ultrastructural dendritic spine remodelling became significant. These changes included a reduction in thin dendritic spines, an increase in mushroom spine head volume, a decrease in smooth endoplasmic reticulum-containing spines, and an increase in dendritic branching. In conclusion, impaired striatal dopaminergic neurotransmisson diminishes striatal synaptic plasticity, which can be partially restored through complex structural changes in striatal spines. These adaptations might represent fundamental homeostatic mechanisms regulating synaptic function during the premotor stage of Parkinson's disease.

Parkinson's disease is a neurodegenerative disorder characterised by the progressive degeneration of dopaminergic neurons within the substantia nigra pars compacta (SN_{pc}). This depletes striatal dopamine, ushering in the emergence of motor signs. A cardinal pathological feature of Parkinson's disease is accumulated intracellular inclusions known as Lewy bodies, primarily composed of the α-synuclein (α-syn) protein[1,2]. Significantly, Parkinson's disease clinical manifestations are apparent only when there has been a substantial loss of dopaminergic neurons, typically 50%–60%. Thus, the premotor stage that precedes the overt presentation of Parkinson's disease is critical[3,4]. Elucidating the underlying processes occurring within the nigrostriatal system during this premotor phase is necessary for pursuing strategies to mitigate these neurons' inexorable degeneration.

Recent evidence highlights the synapse's critical role, particularly at the junction between dopaminergic and striatal neurons, showing that the synapse is where the pathological processes lead to dopaminergic degeneration in Parkinson's disease[5–9]. The striatum, a central component of the basal ganglia, is primarily comprised of GABAergic spiny projection neurons (SPNs), with many residing in the dorsal motor circuit region, which is essential for motor control[10]. These SPNs are distinguished by their dense dendritic spines, which receive inputs from dopaminergic and glutamatergic

[1]Neuroscience Programme, Centre for Applied Medical Research (CIMA), Universidad de Navarra, Pamplona, Spain. [2]Neuroscience Department, University of the Basque Country (UPV/EHU), Leioa, Spain. [3]Ben Towne Center for Childhood Cancer and Blood Disorders Research, Seattle Children's Research Institute, Seattle, USAWA. [4]Weill Institute for Neurosciences, University of California, San Francisco (UCSF), San Francisco, CA, USA. [5]Department of Molecular Biology, Centro de Biología Molecular Severo Ochoa, Consejo Superior de Investigaciones Científicas - Universidad Autónoma de Madrid (CSIC-UAM), Madrid, Spain. [6]Universidad de Málaga, IBIMA- Plataforma BIONAND, Facultad de Medicina, Málaga, Spain. [7]HM CINAC (Centro Integral de Neurociencias Abarca Campal), Hospital Universitario HM Puerta del Sur, HM Hospitales, Madrid, Spain. [8]Instituto de Investigación Sanitaria HM Hospitales, Madrid, Spain. [9]Facultad HM de Ciencias de la Salud de la Universidad Camilo José Cela, Madrid, Spain. [10]Centro de Investigación Biomédica en Red de Enfermedades Neurodegenerativas (CIBERNED), Instituto de Salud Carlos III, Madrid, Spain. [11]Center for Early Relational Health, Columbia University Irving Medical Center, New York, NY, USA. [12]Neurodegeneration and Neuroinflammation Research Group, Institut d'Investigació Biomèdica de Girona Josep Trueta (IDIBGI), Salt, Spain. [13]Navarra Institute for Health Research (IdiSNA), Pamplona, Spain. [14]Neurology Department, Clínica Universidad de Navarra, Pamplona, Spain. [15]These authors contributed equally: Ana Quiroga-Varela, María Cruz Rodríguez-Oroz. ✉e-mail: mcroroz@unav.es

axons, creating a complex synaptic milieu[5,9,11–14]. Dendritic spines play a critical role in synaptic integration and plasticity, but the complexities of dendritic tree branching are equally important for processing synaptic inputs. Together, they contribute to efficient inter-neuronal communication and influence neural activity and behavior. Maintaining normal neural motor circuit function at the synaptic level is a dynamic process primarily regulated by the intricate interplay between dopamine and glutamate within various mechanisms of synaptic plasticity. Disruptions here profoundly affect motor coordination, learning and other striatal-related functions, making them particularly relevant to the study of Parkinson's disease[15].

Striatal synaptic plasticity comprises various types. Synaptic potentiation demonstrates Hebbian plasticity in response to the repeated firing of interconnected neurons. Plasticity is regulated by dopamine and glutamate's modulatory and excitatory activities, respectively. Together, their actions shape synaptic connections, promoting motor learning and skill acquisition[16]. Long-term potentiation (LTP) and long-term depression are prominent manifestations of this plasticity[17].

In contrast, homeostatic plasticity mechanisms primarily focus on stabilising synaptic activity to keep it within a functional range. Typically, this involves fine-tuning the number and sensitivity of receptors, adjusting neurotransmitter release, and other processes aimed at averting excessive excitation or inhibition[18–22]. While many studies have demonstrated abnormal striatal synaptic plasticity in advanced stages of dopaminergic degeneration[14,23–26]; only one study has demonstrated a lack of LTP induction in SPNs, which was correlated with reduced striatal dopamine release before motor sign onset in a mouse model of intrastriatal α-syn fibril inoculation[14].

Synaptic function relies on the structural plasticity of dendritic spines. Much of our current understanding of changes in striatal synaptic morphology in Parkinson's disease originates from studies that used neurotoxin-induced animal models[27–33] and post-mortem analyses of brain tissue obtained from the brains of patients with advanced Parkinson's disease[34–36]. They reported extensive dopaminergic degeneration with diminished dendritic spines with altered morphology of dendrites. Unfortunately, no past studies examined potential structural alterations in striatal dendritic spines and dendritic trees during early-stage dopaminergic loss. Thus, there is a critical need to explore functional and morphological striatal synaptic alterations in early-stage Parkinson's disease.

Our research group previously reported on the stepwise progression of functional and structural alterations at a pre-synaptic level in the striatal synapses[5]. These changes precede symptomatic dopaminergic cell death in a rat model of progressive parkinsonism induced by overexpression of an adeno-associated viral vector (AAVs) coding for A53T mutated human α-syn (hα-syn) in the SN_{pc}. We previously reported that the pathological process begins with deregulated proteins related to energy metabolism and synaptic vesicle cycling. These actions disrupt mitochondrial bioenergetics, reduce dopaminergic terminals, induce ultrastructural changes (e.g. pathological conformation with swollen and bulging morphology), and accumulate autophagic/endocytic vesicles in remaining dopaminergic fibres. Importantly, striatal glutamatergic synapse changes, which account for structural plasticity, emerge before motor abnormalities[5].

This study sought to elucidate the temporal sequence of early functional, synaptic plasticity, and structural changes in the post-synaptic compartment—particularly in the dendritic spines of striatal SPNs—that precede symptomatic dopaminergic cell death. We used the same rat model of progressive parkinsonism through A53T mutated hα-syn overexpression. We assessed these changes at various time points post-inoculation (72 h, 1, 2, and 4 weeks) of the AAV in the SN_{pc}, using a multifaceted functional-structural approach.

Results

Overexpressing hα-syn in the SN_{pc} caused dopaminergic degeneration without motor impairment, confirming the role of the premotor phase

We validated the overexpression of hα-syn in all A53T-hα-syn AAV-inoculated rats and the absence of protein expression in the EVV control animals, consistent with our prior findings (Supplementary Fig. 1)[5]. In the hα-syn group, there was a significant bilateral loss of dopaminergic TH^+ neurons in the SN_{pc} (16% cell loss vs. EVV, $P < 0.05$; Fig. 1B, C), and significantly decreased TH^+ expression within DLS fibres (25% expression loss, $P < 0.01$; Fig. 1B, D) compared to the EVV group at 4 w p.i., wherein the remaining dopaminergic fibres exhibited swelling and bulging ($P < 0.001$; Fig. 1B, E). Additionally, in line with these results, the DAT analysis revealed a mild depletion of dopaminergic fibers in the hα-syn group at 4 weeks post-inoculation, further supporting the nigrostriatal alterations ($P < 0.05$; Fig. 1B, G). This dopaminergic degeneration was not associated with motor impairment as no significant alterations in distance and % time moving in the OFT were observed in hα-syn animals (Fig. 1F).

Overexpression of hα-syn in the SN_{pc} causes early dopamine content changes and LTP impairment in striatal synapses

Striatal dopamine content significantly decreased starting at 72 h p.i. ($P < 0.01$ at 72 h p.i. and $P < 0.05$ at 1 w and 4 w p.i.; Fig. 2A), whereas striatal glutamate levels were unchanged at all examined time points (Fig. 2B).

We assessed synaptic plasticity in isolated striatal synapses using FASS-LTP (Fig. 2C). The hα-syn group exhibited a significant lack of cLTP induction at 72 h p.i. ($P < 0.001$; Fig. 2E) and 1 w p.i. ($P < 0.05$; Fig. 2E) with a trend towards lack of cLTP induction at 4 w p.i. ($P = 0.051$; Fig. 2E) compared to the EVV group (mean values 115.10 ± 11.18 vs. 168.2 ± 15.69 at 4 w p.i. in hα-syn and EVV, respectively; Fig. 2D, E). No differences in baseline GluA1/Nrx1β levels were observed between groups and time points (Supplementary Fig. 2A–C). Similar calcein staining levels were detected in synaptosomes from both groups under baseline conditions and following cLTP stimulation (Supplementary Fig. 2D), confirming the viability of the isolated synaptosomes.

Dendritic spine loss and remodelling in striatal SPNs align with the onset of dopaminergic degeneration despite the lack of motor signs

We examined 66,308 individual dendritic spines (Fig. 3A, B and F) at 1 w and 2 w p.i. and found no discernible changes in spine density, shape, or morphology (head volume, neck length and diameter) across the entire spine population (Fig. 3D, Supplementary Fig. 3A). However, at 4 w p.i., the hα-syn group showed a significant reduction in total spine density compared to the EVV group ($P < 0.01$; Fig. 3D). Subsequent analysis of the morphological subtypes at this time point (Fig. 3C) revealed a significant reduction in overall spine density within thin spines ($P < 0.01$ vs EVV group; Fig. 3E, Supplementary Fig. 4). Regarding spine morphology, the hα-syn group showed significantly larger spine head volumes than the EVV group at 4 w p.i. ($P < 0.01$; Fig. 3D); this was significant only in mushroom spines ($P < 0.05$ vs EVV group; Fig. 3E). While no statistical differences were observed in spine neck length and neck diameter between groups across the entire spine population at any time point (Supplementary Fig. 3A), in the hα-syn group, the neck length of mushroom spines was increased and decreased at the 1 w and 2 w p.i. time points, respectively ($P < 0.05$ vs. EVV; Supplementary Fig. 3B).

Ultrastructural changes in the dendritic spine SER precede motor signs and occur with significant dopaminergic degeneration

The ultrastructural analysis of the smooth endoplasmic reticulum (SER), a vital organelle involved in intracellular calcium regulation, was observed within a subset of 569 dendritic spines out of 2825 spines analysed (Fig. 4A–C). A significant reduction in the proportion of SER^+ spines ($P < 0.01$; Fig. 4D) and a significant increase in the area occupied by SER relative to the total area of the spine head ($P < 0.01$; Fig. 4E) was observed in the hα-syn group vs. the EVV group only at 4 w p.i. Additionally, we observed a non-significant trend between the percentage of SER^+ spines and striatal TH^+ expression ($r = 0.507$; $P = 0.055$; Fig. 4F). Conversely, a significant negative correlation was observed between the SER area to total spine head area ratio and TH expression ($r = -0.744$; $P < 0.05$; Fig. 4G).

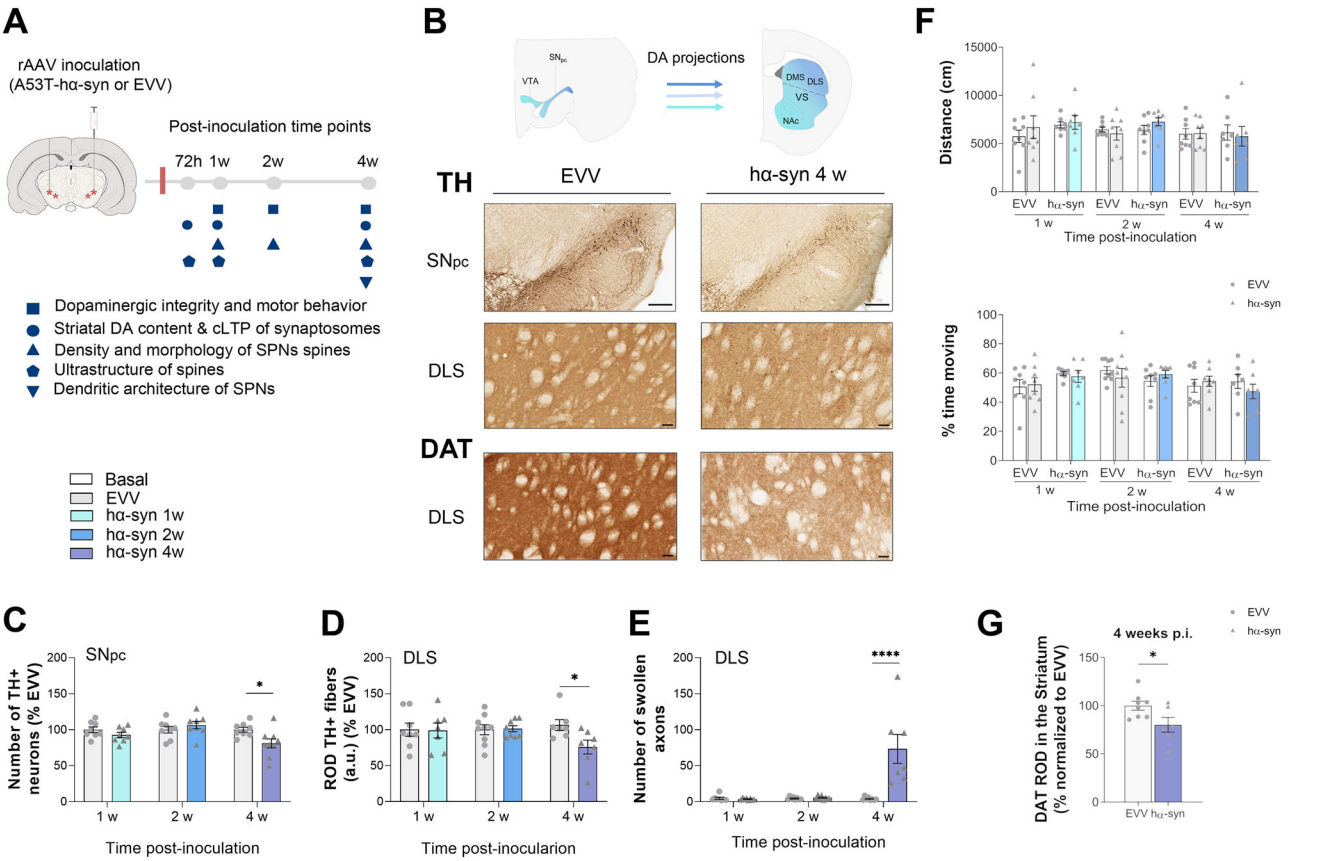

Fig. 1 | Evaluation of motor behaviour and dopaminergic integrity during the premotor stage of the animal model of progressive parkinsonism. A Schematic representation of the viral vector inoculation site (red asterisks, bilaterally in the SN_{pc}) and the experimental design indicating the evaluated post-inoculation (p.i.) time points. **B** Schematic representation of the dopaminergic projections from the SN_{pc} to the striatum in the rat brain (left). The ventrolateral region of the SN_{pc} projects to dorsal areas of the striatum (motor striatum), mainly to the dorsolateral striatum (DLS), while caudomedial SN_{pc} neurons project to the ventral and medial parts of the striatum (associative and limbic striatum). Representative photomicrographs of TH^+ staining in coronal sections of the SN_{pc} and the striatum from animals that received EVV or hα-syn inoculation assessed at 4 w p.i. Scale bars: 300 µm (nigral sections) and 100 µm (striatal sections) showing pathological TH^+ terminal swellings and thickening of fibres at 4 w p.i. in the striatum of the hα-syn group. Representative photomicrographs of DAT staining in coronal sections of the SN_{pc} and the striatum from animals that received EVV or hα-syn inoculation assessed at 4 w p.i. Scale bars: 100 µm. **C** Number of TH^+ neurons in the SN_{pc} normalised to the corresponding EVV group. **D** Relative optical density (ROD) analysis of TH expression in the dorsolateral striatum normalised to the corresponding EVV group. **E** Number of swollen TH^+ axons in the dorsolateral striatum of hα-syn and EVV groups. Values are presented as the mean ± SEM ($n = 7–9$ for each group and time point; Two-way ANOVA followed by Sidak post-hoc test: $^*P < 0.05$, $^{****}P < 0.0001$). **F** Open field test for evaluating locomotor activity before surgery (baseline) and at 1, 2 and 4 w p.i. in EVV and hα-syn inoculated animals. Box plots showing the distance (cm) and % of the time moving ($n = 7–9$ for each group and time point; Two-way ANOVA for repeated measures: no statistical differences). Abbreviations: a.u., arbitrary units; DLS, dorsolateral striatum; DMS, dorsomedial striatum; NAc, nucleus accumbens; VS, ventral striatum; VTA, ventral tegmental area. **G** Relative optical density (ROD) analysis of DAT expression in the dorsolateral striatum normalised to the corresponding EVV group.

During the premotor phase, striatal SPNs display increased dendritic complexity and branching alongside significant nigrostriatal degeneration

We investigated morphological changes in dendritic arbour complexity and striatal SPNs associated with dopaminergic degeneration at the 4 w p.i. time point (Fig. 5A). Our initial Sholl analysis revealed a significant increase in the number of dendritic tree intersections in the hα-syn group ($P < 0.05$; Fig. 5B). A subsequent examination of SPN dendritic morphology revealed a significant increase in the number of dendritic branch points and terminal branches in the hα-syn group ($P < 0.01$ vs. EVV; Fig. 5C); however, we did not observe significant differences in total dendritic length (Fig. 5C). There was a trend towards a negative correlation between the number of terminal branches and striatal TH^+ expression ($r = -0.613$; $P = 0.059$; Fig. 5D).

Discussion

We investigated the temporal sequence of functional (synaptic plasticity) and post-synaptic morphological (dendritic spine morphology) changes in SPNs from the dorsolateral striatum. To accomplish this, we induced dopaminergic dysfunction in the striatum before the onset of parkinsonian motor features using a model of progressive parkinsonism induced by nigral inoculation of AAV-A53T-hα-syn (Fig. 6).

Our findings reveal that hα-syn overexpression in the SN_{pc} reduces dopamine concentrations at 72 h p.i. While not directly indicative of release dynamics, these data offer valuable insights into the total levels of neurotransmitters available for release. These findings can also be integrated with prior microdialysis studies in the same animal model and at comparable time points[37], which confirmed dopamine dysregulation from early stages in this model. The reduction in striatal dopamine content at the earliest time point underscores the chronic nature of dopaminergic loss in this model. We observed sustained reductions in cLTP at 72 h and 1 w p.i. before dopaminergic degeneration became significant at 4 w p.i. At this time, a partial recovery of cLTP and a shift in spine remodelling were observed. Specifically, we observed reduced thin spine density, mushroom spine head enlargement, increased SER^+ area, and enhanced dendritic branching and intersections. These changes are evidence of dynamic post-synaptic architecture reshaping and structural adaptations within the motor striatum's

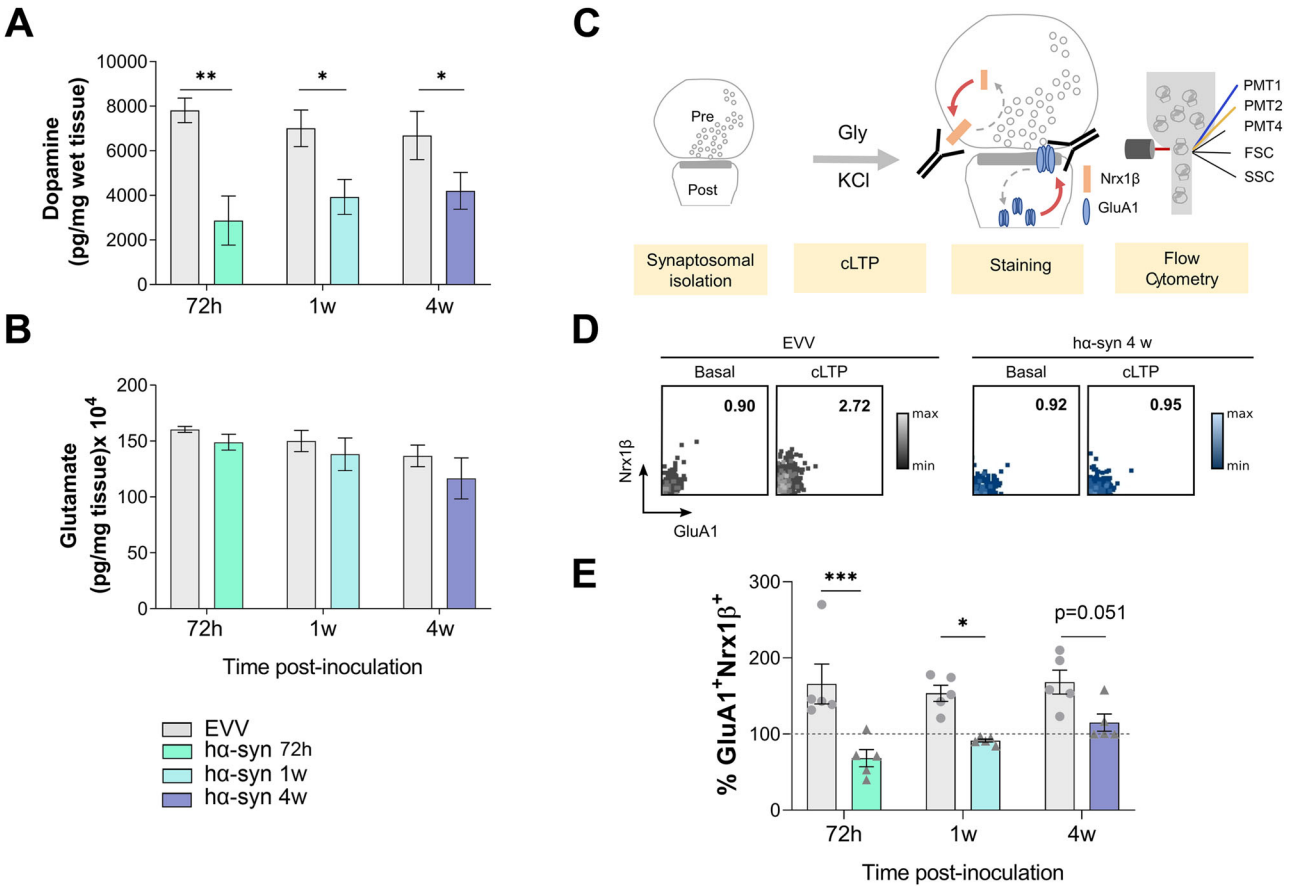

Fig. 2 | Early synaptic deficits in the striatum of hα-syn overexpressing animals. **A** Dopamine and **B** Glutamate levels in the striatum from EVV and hα-syn groups. Values are presented as the mean ± SEM ($n = 5$–10 animals for each group and time point). Two-way ANOVA followed by LSD post-hoc test: $^{*}P < 0.05$, $^{**}P < 0.01$. **C** FASS-LTP workflow overview. Isolation of crude synaptosomes is followed by glycine (Gly)-KCl stimulation (cLTP) and immunolabeling for surface GluA1 and Nrx1β. Flow cytometry identifies potentiated synapses by size and extracellular GluA1+Nrx1β^{+} double staining. **D** Representative GluA1-Nrx1β plots showing percentage GluA1+Nrx1β^{+} events in synaptosomes from EVV and hα-syn groups at 4 w p.i. **E** Percentage GluA1+Nrx1β^{+} double staining events normalised to synaptosomes maintained in the baseline state. Data are shown as mean ± SEM ($n = 5$ per group and time point). Two-way ANOVA followed by Sidak post-hoc test: $^{*}P < 0.05$, $^{***}P < 0.001$. PMT photomultiplier tube, FSC forward scatter, SSC side scatter.

neuronal network that precede the onset of motor dysfunction. These results suggest sequential triggering of post-synaptic homeostatic mechanisms in the striatum by dopaminergic dysfunction and degeneration. These changes partially restore synaptic strength and support a compensatory neural motor circuitry response to maintain functional integrity.

Understanding the complex functional and structural changes in areas of the brain affected during the premotor stages of Parkinson's disease is crucial for developing effective interventions to maintain systemic integrity while delaying neurodegeneration and clinical disease expression[4]. However, while extensive research has explored functional and structural changes in striatal SPNs in advanced Parkinson's disease stages[16,36,38–42], little is known about the premotor phase.

In line with what we described at the pre-synaptic level[5], synaptic functional alterations antedate morphological changes in the striatum's post-synaptic compartment. Failure of synaptic plasticity (lack of cLTP induction) occurs once the dopamine concentration is sufficiently reduced and well before dopaminergic degeneration. These observations suggest that hα-syn overexpression in dopaminergic cell somas of the SN_{pc} regulates dopamine content in striatal synapses.

Interestingly, the animals' glutamate levels remained unaffected, probably due to the complex ultrastructural remodelling in glutamatergic synapses within the dorsal striatum, similar to what was shown in our previous work[5]. These are all evidence of compensatory glutamatergic activity[31,43–45] and indicate that initial disruption of the balance between excitatory glutamatergic and modulatory dopaminergic neurotransmission is sufficient to disrupt normal synaptic plasticity. However, at 4 w p.i.—and without changes in the dopamine and glutamate concentration compared to the previously analysed time points—there is a partial recovery of striatal cLTP even in the context of significant dopaminergic denervation. This recovery points to potential synaptic plasticity mechanisms capable of counteracting the effects of neurodegeneration at this time point. Importantly, induction of cLTP compared to basal levels discards saturation of synaptic strength due to prior potentiation.

These changes occur alongside marked morphological changes in the post-synaptic compartment in striatal SPNs, particularly in dendritic spine dynamics. Fluctuations in spine neck length within mushroom spines and changes in thin spine density and mushroom spine head size suggest neurons' dynamic response to optimise synaptic function amidst altered dopaminergic levels, as supported by previous research[46,47]. These structural adjustments likely compensate for fluctuations in dopaminergic signalling. Changes in synaptic strength—including alterations in spine head size and conversions between thin and mushroom spines[48,49]—help preserve synaptic function and neuronal communication. The observed decrease in thin spine density and enlargement of mushroom spine heads at 4 w p.i. may indicate a shift towards synapse stabilisation or strengthening[50]. These changes reflect compensatory mechanisms that preserve synaptic function, as evidenced by the partial recovery of cLTP by 4 w. The partial recovery of dopamine release and the lack of motor deficits at 4 weeks, despite notable dopaminergic loss, can be attributed to these structural and functional adaptations, which maintain neuronal connectivity and motor activity.

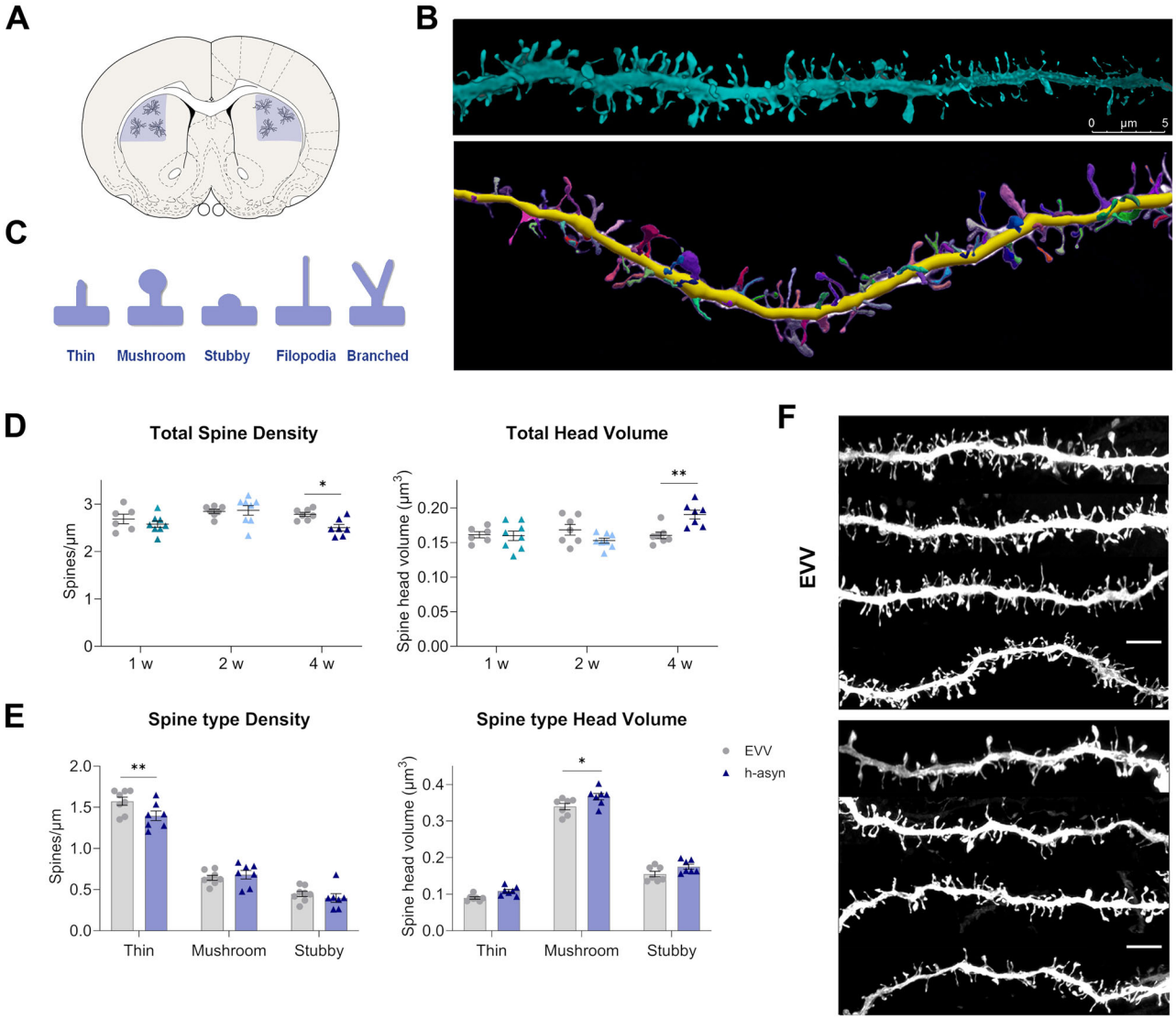

Fig. 3 | SPNs dendritic spine loss and spine head remodelling only when dopaminergic neurodegeneration occurs. A Representation of the brain section and the dorsolateral striatum area (blue) where SPNs were microinjected. **B** Representative 3D high-resolution photomicrographs of dendritic segments and detected dendritic spines using Neurolucida 360 (bottom). **C** Schematic representation of classified dendritic spine types: thin, mushroom, stubby, filopodia, and branched. **D** Total dendritic spine density (left) and total dendritic spine head volume (right) of SPNs from the dorsolateral striatum of EVV and hα-syn groups. Data are presented as mean ± SEM (n = 6–8 animals per group and time point). Two-way ANOVA followed by Sidak post-hoc test: $^{*}P < 0.05$; $^{**}P < 0.01$. **E** Density (left) and head volume (right) of thin, mushroom and stubby spine subtypes in EVV and hα-syn groups at 4 w p.i. Data are presented as mean ± SEM (n = 6–8 animals per group and time point). Two-way ANOVA followed by Sidak post-hoc test: $^{*}P < 0.05$; $^{**}P < 0.01$. **F** Representative dendritic segments from EVV and hα-syn groups at 4 w p.i. Scale bars: 5 µm.

These dynamic adjustments underscore the complex interplay of homeostatic mechanisms and highlight the brain's resilience during the early stages of Parkinson's disease. Post-synaptic adaptations, in particular, play a critical role in maintaining synaptic strength and motor function. Understanding these compensatory responses could inform strategies to delay motor signs through early interventions targeting synaptic plasticity and neurotransmitter balance.

We observed increased dendritic complexity (branch points and terminal branches) and altered SER organisation at 4 w p.i., further evidence of compensatory changes in dendritic morphology. As dendritic complexity increased, we observed a tendency towards an inverse correlation between terminal branches and TH^{+} expression. These results suggest a compensatory mechanism that enhances synaptic efficiency by facilitating more contacts between whatever dopamine terminals remain and SPNs. These findings agree with prior research findings regarding the stability of the dendritic arbour trees under varying dopamine levels that suggest a consistent compensatory response to help maintain synaptic function despite dopaminergic changes[51,52]. The trend towards an inverse correlation between terminal branches and TH^{+} expression highlights the crucial role of dendritic morphology in modulating synaptic connectivity within the basal ganglia circuitry, once again corroborating previous findings[53].

Our study on SER organisation revealed a progressive loss of SER^{+} spines, consistent with previous findings of downregulated calcium channels. Dopamine depletion may lead to prolonged intracellular calcium increases in SPNs, contributing to previously described excitotoxic processes[41,54,55]. This vulnerability is supported by an observed increase in the SER area within dendritic spine heads, which affects intracellular calcium buffering[56]. There is likely a link between increased calcium buffering and changes in spine structure, as evidenced by (and potentially contributing to) observed spine loss at 4 w p.i. Conversely, surviving SER^{+} spines showed expanded spine apparatus, possibly enhancing signal

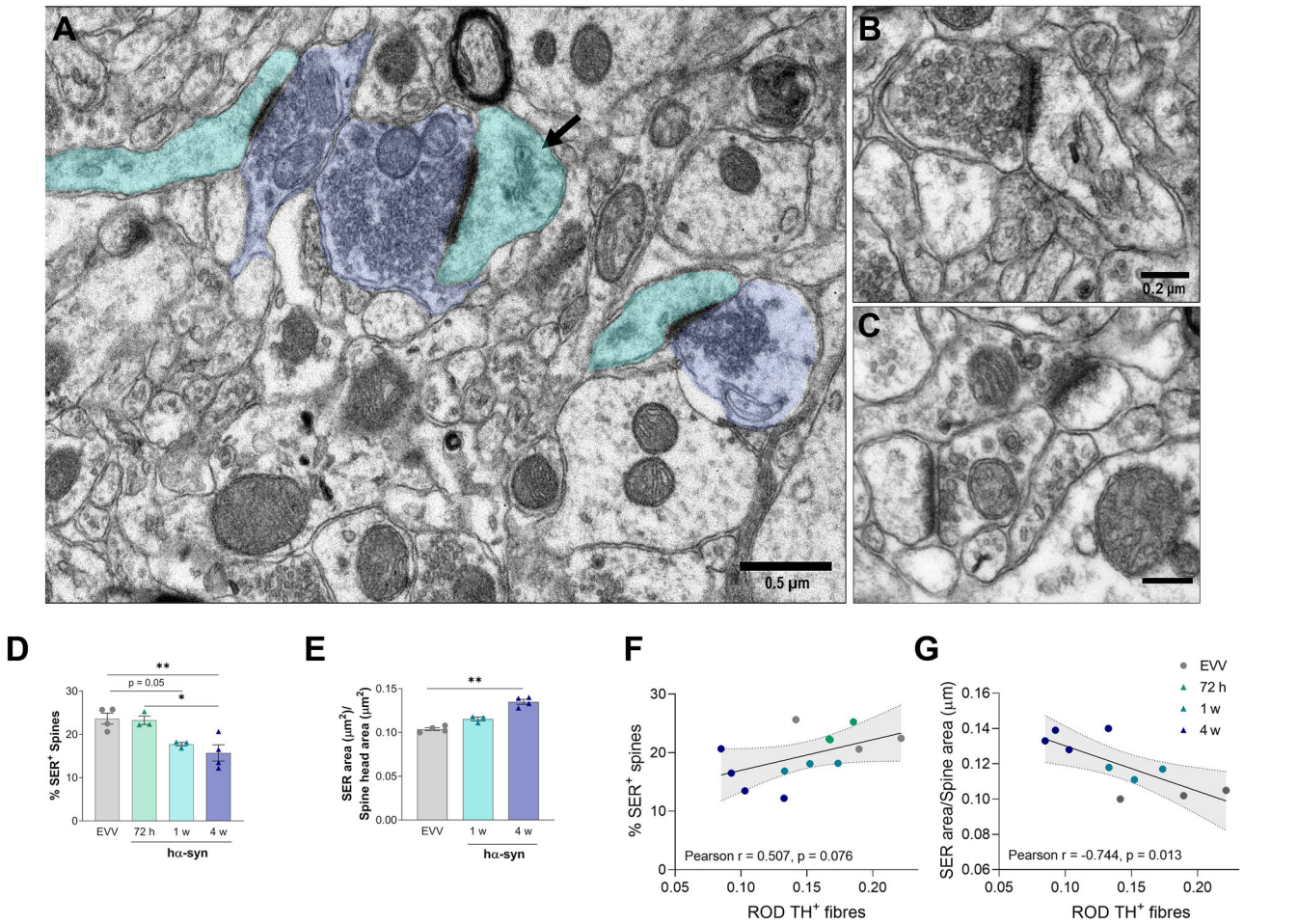

Fig. 4 | Progressive ultrastructural changes in the SER inside dendritic spines of SPNs. A Electron microscopy photomicrograph of the dorsal striatum showing excitatory synapses composed of pre-synaptic terminals (blue) and post-synaptic dendritic spines (turquoise). The SER is marked with an arrow. Scale bar: 0.5 µm. **B** Electron microscopy photomicrograph showing a dendritic spine from an SPN with SER in the head and **C** Dendritic spines without SER. Scale bar: 0.2 µm. **D** Percentage of dendritic spines with SER in the dorsal striatum of EVV and hα-syn groups. **E** Ratio of the area occupied by the SER concerning the spine head area of EVV and hα-syn groups. Data are presented as mean ± SEM ($n = 3–4$ per group and time point). Kruskal-Wallis test followed by uncorrected Dunn's post-hoc test: $^{*}P < 0.05$; $^{**}P < 0.01$. **F** Scattered diagrams showing the correlation of the percentage of SER^{+} spines with the striatal TH ROD ($P = 0.076$). **G** The ratio of the area occupied by the SER concerning the spine head area with the striatal TH ROD ($P = 0.013$). Pearson's correlation. ROD relative optical density, s dendritic spine, t pre-synaptic terminal.

potentiation and sustaining and enlarging synapses to maintain overall synaptic function amidst dopaminergic neurodegeneration[57]. However, it is important to note that the exact nature of these changes—whether excitotoxic or compensatory—remains uncertain. Further investigations are needed to delineate the precise role of SER alterations in the context of parkinsonism-associated spine remodelling.

One limitation of our study is that the time points analysed may incompletely capture dynamic, longitudinal changes in spine dynamics. Still, we studied critical time points according to the changes in premotor dopamine levels and dopaminergic degeneration. Future studies could extend this observation period to yield a more comprehensive understanding of synaptic changes in Parkinson's disease. Our functional studies were also conducted on isolated striatal synaptosomes with diverse neurotransmitter profiles, which prevented the isolation of specific synaptosome populations. This necessitates staining for surface markers and additional processing time, which could impact synaptosome viability and the assessment of cLTP functionality[58,59].

The understanding of synaptic changes during the premotor stages of Parkinson's disease is crucial for developing interventions aimed at delaying neurodegeneration and maintaining neuronal function that could delay or even prevent the onset of motor signs. Our findings, showing alterations in synaptic plasticity and structural remodeling of dendritic spines, provide critical insight into the earliest stages of parkinsonism. These changes precede the substantial loss of dopaminergic input and motor signs and may correspond to the premotor phase in human Parkinson's disease. This model may thus provide a platform to test the efficacy of interventions aimed at restoring dopaminergic function or enhancing synaptic plasticity in the earliest phases of disease. This would not only enable earlier treatment but also offer the potential to slow disease progression through interventions targeting synaptic dysfunction. For instance, pharmacological targeting of signalling pathways such as BDNF-TrkB, eEF2-kinase, retinoic acid, or vesicle trafficking pathways (previously explored in other synaptopathies[60]) could help restore synaptic function in Parkinson's disease. BDNF-TrkB signalling is essential for synaptic strength and plasticity in the striatum, and its modulation may counteract synaptic disruptions. Enhancing this pathway or inhibiting factors that compromise synaptic integrity, such as eEF2-kinase, could slow disease progression and support neuronal health in early Parkinson's disease stages. Thus, restoring synaptic strength and preventing structural changes could enhance compensatory responses in neural circuitry, providing new therapeutic avenues for Parkinson's disease that might help delay motor sign onset and improve patients' overall quality of life.

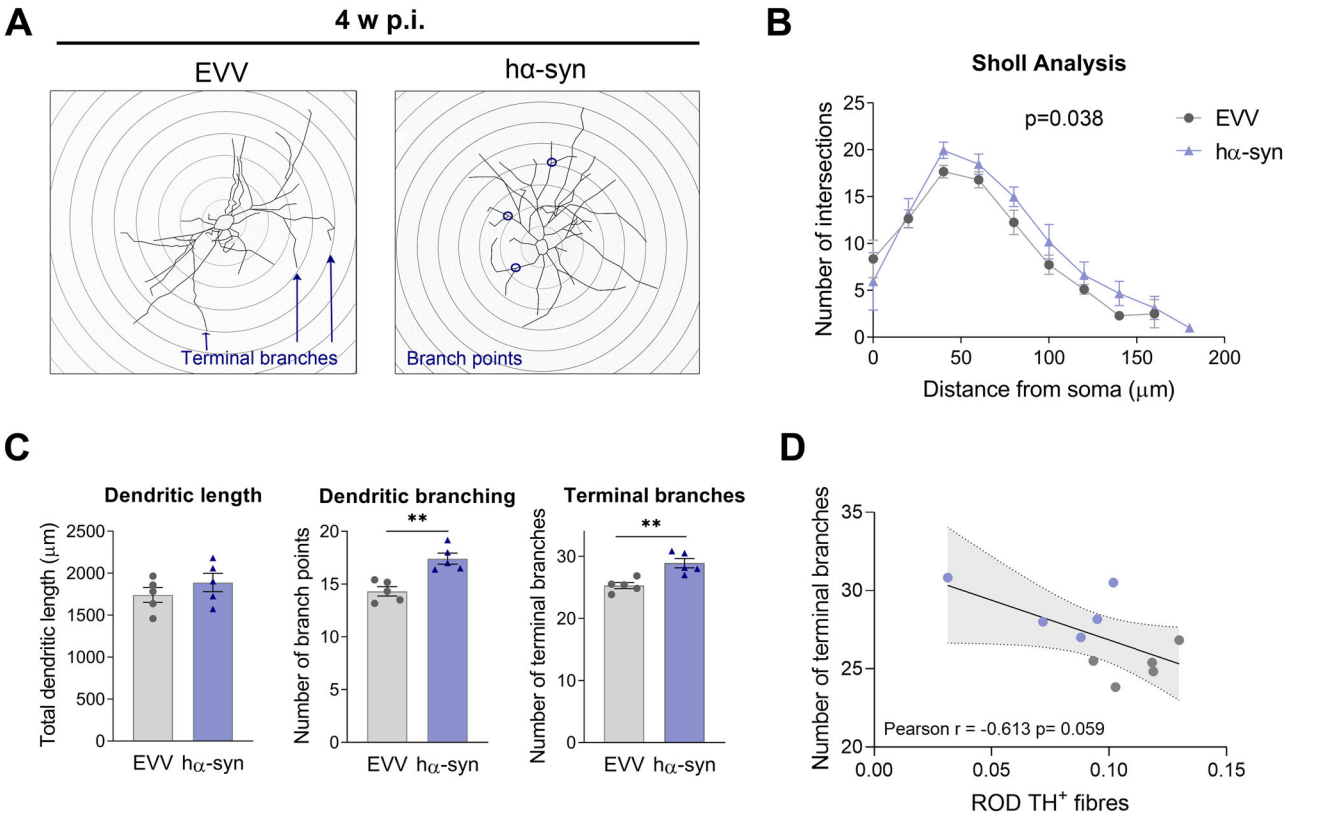

Fig. 5 | Dendritic complexity and branching of SPNs are increased at 4 w p.i. **A** Representative tracings of striatal SPNs showing Sholl crossings every 20 μm from EVV and hα-syn animals. Representative terminal branches are depicted as blue arrows and dendritic branch points as blue circles. **B** Number of intersections at specified distances from the soma in the EVV and hα-syn groups. Data are shown as mean ± SEM ($n = 5$ per group). Paired t-test: $P = 0.038$. **C** Total dendritic length (left), total dendritic branching (middle) and terminal branches (right) of EVV and hα-syn groups. Data are shown as mean ± SEM ($n = 5$ per group). Unpaired t-test: $^{**}P < 0.01$. **D** Scattered diagrams showing the correlation of the number of terminal branches with the striatal TH ROD ($P = 0.059$). Pearson's correlation. ROD relative optical density.

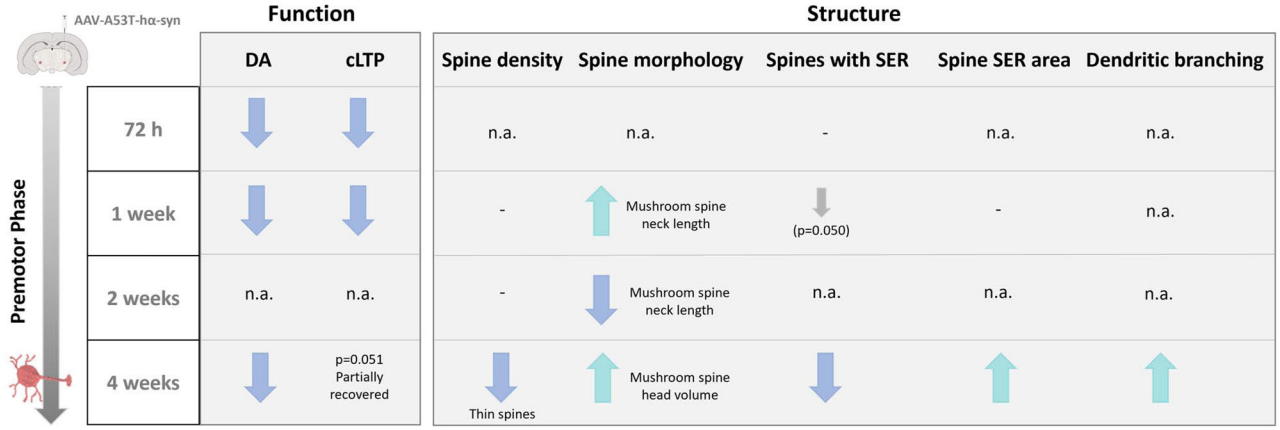

Fig. 6 | Summary of the main results obtained in this study for striatal function and SPN structure at different AAV-A53T-hα-syn post-inoculation time points. Significant increases are shown in turquoise and significant decreases in blue compared to the corresponding EVV group. Nigrostriatal pathway neurodegeneration was not evident until 4 w p.i. The hα-syn expression was apparent in the SN_{pc} beginning at 72 h p.i. DA dopamine, cLTP chemical long-term potentiation, n.a. not available.

Collectively, our results highlight the dynamic interplay between early dopaminergic dysfunction and post-synaptic compensatory mechanisms during the initial phase of dopamine deficiency. Importantly, hα-syn overexpression in the SN_{pc} led to a dopaminergic deficiency, disrupting synaptic plasticity (cLTP). Subsequently, partial restoration was observed due to post-synaptic morphological homeostatic responses. Such responses —including changes in spine density, mushroom spine morphology, spine SER adaptation and dendritic branching—underscore the brain's resilience and ability to maintain synaptic strength to ensure proper transmission and integration of motor information during the premotor stage of Parkinson's disease. Our results may inform future therapies to restore synaptic plasticity to rescue synaptic function in the early stages of Parkinson's disease.

Methods

Animals

Adult male Sprague-Dawley rats (325–350 g) were obtained from Charles River Laboratories (Boston, MA, USA). The animals were maintained in a room with standard temperature and humidity (70% humidity, 22 °C) on a regular 12 h light/dark cycle, with food and tap water permitted *ad libitum*. All the experimental procedures were approved by the animal research committees of CIMA-Universidad de Navarra (107-17; Pamplona, Spain) and were carried out in strict accordance with the guidelines of the Spanish Government (RD53/2013) and the European Union Council Directive (2010/63/EU) on the protection of animals used for research purposes. All efforts were made to minimise animal suffering and minimise the number of animals used.

Animal model and experimental design

Recombinant AAVs with AAV2/9 serotype were custom ordered from the vector core facility at the University of Bordeaux (Bordeaux, France). The hα-syn group was inoculated with the viral vector AAV2/9-CMV-WPRE-hα-synA53T, which overexpresses the hα-syn with the A53T mutation (8×10^{12} genomic particles/ml). The control group was inoculated with the viral vector AAV2/9-CMV-WPRE-EVV and empty AAV capsids without transgene overexpression (EVV group; 2×10^{13} genomic particles/ml).

This cross-sectional study involved two experimental groups (hα-syn and EVV) and multiple independent subgroups of rats evaluated at different post-inoculation (p.i.) time points: 72 h (h), 1 week (w), 2 weeks (w) and 4 weeks (w) (Fig. 1A).

Based on our previous study[5] we conducted FASS-LTP and measured neurotransmitter concentrations in the striatum at the onset of hα-syn overexpression in the SN_{pc} (72 h) and in the striatum (1 w), and when a significant reduction of dopaminergic neurons in the SN_{pc} and dopaminergic terminals in the striatum occurred (4 w). To investigate the structural impact of hα-syn overexpression on the dendritic spines of striatal SPNs, we quantitatively analysed dendritic morphology and arborisation following the start of hα-syn overexpression in the striatum (at 1, 2 and 4 w p.i).

For FASS-LTP and HPLC analyses, 5–10 animals per group were used at each time point (72 h, and 1 and 4 weeks p.i.) (Fig. 1A). For the open field test, high-resolution morphometric dendritic spine analysis, and corresponding immunohistochemical studies, 7–9 animals per group were examined at 1, 2, and 4 w p.i. The SPN dendritic complexity study included 5 animals per group at 4 w p.i. Lastly, for the electron microscopy (EM) study, 3–4 animals per group were analyzed at different hα-syn time points (72 h, and 1 and 4 w p.i.).

Stereotaxic surgery

The rats were anesthetised with isoflurane in air enriched with 1%–2% oxygen and placed in a stereotactic head frame (Stoelting, Wood Dale, IL). The corresponding AAVs were injected bilaterally into the SNpc (1 µl per site, 0.2 µl/min)[5]. The Bregma coordinates were (1) anteroposterior −4.9, lateral ±2.2, ventral −7.7 mm; and (2) anteroposterior −5.4, lateral ±2.0, ventral −7.7 mm. The injection needle was left in place for 2 min before being slowly retracted from the brain.

Open field test

Spontaneous locomotor activity was assessed using the open field test (OFT) at baseline and 1, 2, or 4 w p.i. To minimise the likelihood of handling-induced anxiety, the rats were systematically acclimated to the testing room and the experimenter's handling procedures over several days preceding the OFT. Each group of animals ($n = 7–9$ animals for each time point) underwent a single habituation session (15 min) to explore the open arena (1 m length x 1 m width x 60 cm height) under dim lighting one day before the test. The animals were permitted to freely explore the open field while testing (15 min) while being continuously video recorded. We evaluated various behavioural parameters—including the total distance travelled (in cm) and the percentage of time spent in motion—using Ethovision X13 software (Noldus Information Technology, The Netherlands).

Brain tissue collection

Animals from the hα-syn and EVV groups ($n = 5–10$/group at each time point) were euthanised by CO_2 inhalation at the corresponding endpoint p.i. (72 h, 1 and 4 w). Following euthanasia, the rats' brains were rapidly removed, and the striata were promptly dissected and processed. One of the striata was cryopreserved in 320 mM sucrose containing 10 mM HEPES, protease inhibitors (Sigma-Aldrich, St Louis, MO) and phosphatase inhibitors (Thermo Fisher Scientific; Waltham, MA; pH 7.4) as previously described[61] and slowly frozen overnight using a CoolCell Alcohol-Free Cell Freezing Container (Corning) to ensure standardised controlled freezing. This cryopreserved tissue was subsequently stored at −80 °C until homogenisation for functional FASS-LTP studies. The other striatum was frozen on dry ice and stored at −80 °C for subsequent quantification of neurotransmitter levels.

Synaptosome isolation

We isolated the synaptosomes from the cryopreserved striatal tissue as described previously[61,62]. Each striatum was homogenised (6–8 manual strokes in a Glass-Teflon grinder) in 320 mM sucrose (1.5 ml) containing 10 mM HEPES and protease/phosphatase inhibitors mixture with a pH 7.4 (Thermo Fisher Scientific, Waltham, MA). The homogenate was centrifuged at 1200 x g for 10 min, and the resulting supernatant (S1) was centrifuged at 12,000 x g for 20 min. The pellet was resuspended by gently pipetting up and down (10–20 times) in 1.5 ml of extracellular (120 mM NaCl, 3 mM KCl, 2 mM CaCl2, 2 mM MgCl2, 15 mM glucose, 15 mM HEPES, pH 7.4) or cLTP solutions (125 mM NaCl, 2 mM CaCl2, 5 mM KCl, 10 mM HEPES, 30 mM glucose, pH 7.4). The synaptosome P2 fraction was filtered using a 40-µm pore cell strainer (BD Biosciences, Franklin Lakes, NJ) and incubated in a cell culture dish (30 mm) while agitating at room temperature for 10–15 min during recovery[61]. All isolation steps were performed at 4 °C, with materials precooled on ice.

Fluorescence analysis of single-synapse LTP (FASS-LTP)

FASS-LTP, a technique that examines changes in synapses following NMDAR activation by depolarization in the presence of the NMDAR co-agonist glycine[61,62], was assessed by flow cytometry (FACSCanto II System; BD Biosciences, Franklin Lakes, NJ) and FlowJo software (v10; FlowJo; LLC, BD Biosciences, Franklin Lakes, NJ, USA) in isolated single synaptosomes after chemical induction of LTP (cLTP) and fluorescent staining of presynaptic Nrx1β and post-synaptic GluA1 AMPAR subunit.

FASS-LTP focuses on inserting AMPA glutamate receptors (AMPARs) into the postsynaptic membrane, a key event in the potentiation of synaptic transmission[61]. After chemical induction of long-term potentiation (cLTP), the activity-dependent increase in surface GluA1-containing AMPARs is quantified using flow cytometry in isolated synaptosomes. Potentiated synapses are identified by extracellular labeling of two key markers: GluA1, which represents postsynaptic AMPARs, and neurexin-1β (Nrx1β), a presynaptic adhesion molecule stabilized at the membrane by synaptic activity. This dual labelling of GluA1 and Nrx1β enables the identification of synaptosomes that contain both pre- and postsynaptic elements, offering a robust means to study synaptic potentiation[61,62]. Furthermore, this approach enhances the accuracy of detecting potentiated synapses, ensuring a robust and high-fidelity assessment of synaptic activity.

Isolated synaptosomes were maintained in cLTP solution (125 mM NaCl, 5 mM KCl, 2 mM CaCl2, 30 mM glucose and 10 mM HEPES; pH 7.4) or external solution (120 mM NaCl, 3 mM KCl, 2 mM CaCl2, 2 mM MgCl2, 15 mM glucose and 15 mM HEPES; pH 7.4) as control condition, and subsequently incubated in a cell culture dish (30 mm) with agitation at room temperature for 10-15 min for recovery and transferred to cytometry tubes (180 µl). Synaptosomes in cLTP solution were incubated with glycine (5 mM glycine in cLTP solution freshly supplemented with 0.01 mM strychnine and 0.2 mM bicuculline methiodide). The external solution was added to the synaptosomes in basal condition and then incubated for 15 min at 37 °C. Next, the synaptosomes in the cLTP solution were stimulated using a high KCl concentration solution (50 mM NaCl, 2 mM CaCl2, 100 mM

KCl, 10 mM HEPES, 30 mM glucose, 0.5 mM glycine, 0.001 mM strychnine, 0.02 mM bicuculline methiodide, pH 7.4). The external solution was added to the control synaptosomes and then incubated for 30 min at 37 °C. All stimulation was stopped with ice-cold 0.1 mM EDTA in PBS. Afterwards, samples were blocked with 5% fetal bovine serum in PBS and centrifuged (2500 x g for 10 min; 4 °C). A primary antibody solution containing rabbit anti-GluA1 (1:1,500; Cell Signalling Technology, Danvers, MA, #13185) and mouse anti-Nrx1β (1:400; UC Davis/NIH NeuroMab Facility, #75–216) antibodies and Calcein AM (100 nM; eBioscience Inc, San Diego, CA, #65-0853-39) were added to the resuspended pellet. This solution was incubated for 30 min at 4 °C with agitation. The synaptosomes were washed with ice-cold blocking buffer and centrifuged (2,500 x g for 5 min; 4 °C). A secondary antibody solution containing anti-rabbit Brilliant Violet 421 (1:400; Jackson ImmunoResearch, Philadelphia, PA, #111-675-144) and anti-mouse-Alexa Fluor 647 (1:800; Invitrogen, #A-21240) antibodies and Calcein AM (100 nM) was added to the tubes, which were then incubated for 30 min at 4 °C with agitation. Afterwards, the synaptosomes were washed with PBS, fixed with 0.25% paraformaldehyde (PFA), and stored in the dark at 4 °C. The samples were acquired using a FACSCanto II System (BD Biosciences, Franklin Lakes, NJ). We excluded small fragments and debris by establishing an FSC threshold (gain = 500) and collecting 50,000 size-gated particles. FlowJo software (v10; FlowJo, LLC, BD Biosciences, Franklin Lakes, NJ) was used for all flow cytometry analyses. We initially selected particles with sizes ranging from approximately 0.75 to 3 µm, corresponding to synaptosomes (Supplementary Fig. 2B). We used isolated rat mitochondria (~ 0.5 µm) and nuclei (~ 8 µm) as size references. We then excluded doublets and large aggregates. Calcein AM-positive events were selected using standard staining controls corresponding to functional synaptosomes (Supplementary Fig. 2B). We identified the single-positive populations for GluA1 and Nrx1β and then used the 'Make and Gate' Boolean analysis tool to assess the double-positive population. Using a quad gate, we visually displayed the GluA1 and Nrx1β staining on the same graph (Supplementary Fig. 2B). An increase in the GluA1/Nrx1β double-positive population in cLTP samples compared to the baseline condition indicated cLTP.

High-performance liquid chromatography (HPLC)

Dopamine and glutamate concentrations in the striata of animals in the hα-syn and EVV groups were determined using HPLC with electrochemical detection (DECADE, Antec Leyden, The Netherlands) and a high-sensitivity analytic flow cell (VT-03). The working electrode was set at 0.8 V for dopamine, and we used a column (Spherisorb ODS2 5 mm, 15 ×0.46 mm; Teknokroma, Spain). The working electrode was set at 0.7 V for glutamate, using a column (Biophase ODS 5 mm, 4.6 ×150 mm; Bioanalytical Systems, West Lafayette, USA) that underwent precolumn derivatisation. The results are expressed in pg/mg of wet tissue.

Fixed brain tissue collection for the 3D morphometric study

For high-resolution morphometric and the corresponding immunohistochemical studies, animals ($n = 6–8$/group at each time point) were deeply anesthetised and perfused transcardially with 1% paraformaldehyde (PFA) in 0.1 M PB (pH 7.4) for 1 min followed by 4% PFA in 0.1 M PB (pH 7.4) for 11 min (40 ml/min flow rate)[63]. The brains were quickly removed and post-fixed in 4% PFA in 0.1 M PB, with a pH of 7.4 for 2 h at 4 °C under agitation. Afterwards, the brains were transferred to a preservative solution containing 0.1% sodium azide in PBS (pH 7.4) and stored at 4 °C until their use. The striatum was serially sectioned using a vibratome (VT1000S, Leica Microsystems, Germany) into one 300 µm-thick coronal slice and three 50 µm-thick slices. We used the posterior 300 µm-thick sections of the striatum (approx. +0.2– + 0.7 mm from Bregma)[64] for single-cell intracellular injections. We used 50 µm-thick sections for immunohistochemical studies to confirm the dopaminergic lesion. The whole SN_{pc} was also serially sectioned into 50 µm-thick sections for further immunohistochemical studies.

Immunohistochemistry

As described previously, immunohistochemistry studies were performed on free-floating coronal sections containing the striatum and SN_{pc}[5]. Briefly, tissue was quenched in 3% H_2O_2 and blocked in normal horse serum and 0.2% Triton X-100 (PBS-T). Afterwards, the samples were incubated overnight with the primary antibody mouse anti-TH (1:1.000; Merck Millipore, Burlington, MA, MAB5280). The sections were then incubated for 1 h in an anti-mouse biotinylated secondary antibody (1:500; Vector Laboratories, Burlingame, CA) with avidin-biotin complex (ABC kits; Vector Laboratories, Burlingame, CA). Immunostaining was visualised following a reaction with 3,3-diaminobenzidine (Sigma-Aldrich, St. Louis, MO). The sections were then mounted on glass Superfrost slides (ThermoFisher Scientific, Waltham, MA), dried, dehydrated with graded alcohols, cleared in xylene, and coverslipped with Eukitt® mounting medium (Sigma-Aldrich, St. Louis, MO).

Quantification of TH^+ neurons in the SNpc and striatal TH expression levels

The number of TH^+ neurons in the SN_{pc} was estimated using stereological cell counting with the optical fractionator method since these processes are unaffected by changes in the reference volume of the sampled structure[65]. We used an interactive computer system with an Olympus microscope and a digital camera (Lumenera, MicroBrightField Bioscience, Williston, VT) with Stereo Investigator software for interactive test grid and motorised stage control (MicroBrightField Bioscience, Williston, VT). TH^+ stained neurons were counted in the SN_{pc} throughout the entire rostrocaudal axis of the SN_{pc} (7–8 sections with a 6-section interval). We calculated the total number of TH^+ stained neurons in the SN_{pc} using the formula described by West et al.[66]. The striatal sections were scanned using Aperio ImageScope (Leica Biosystems, Germany). We acquired one image per hemisphere from 3 sections (6 images/animal) at 2x magnification to analyse the striatal TH expression. The resultant images were converted to 8 bits, and the mean optical density of the dorsolateral striatum was analysed using Fiji (NIH, https://fiji.sc/). To assess the abnormal shape of the remaining dopaminergic fibres, we quantified the swollen or bulging appearance of TH^+ axons. To quantify swollen TH^+ axons, 6 images from the dorsolateral striatum (DLS) per section (3 per hemisphere) and 3 sections per animal (18 images/animal) were acquired at 20x.

Images were processed using a custom macro in Fiji (NIH), with the following steps: First, images were converted to 8-bit grayscale and a rolling ball algorithm (rolling = 10) was applied to remove uneven background illumination and highlight axonal structures. Next, the MaxEntropy algorithm was used to determine an intensity threshold separating the axonal structures from the background. Then, the thresholded image was converted to a binary mask, with axonal structures represented as white on a black background, allowing for particle analysis. Particles larger than 12 µm² were identified and quantified as swollen axons, with outlines displayed for visual verification. This automated pipeline ensures consistent and unbiased quantification of swollen TH+ axons across all images. Data were grouped by animal and group (EVV or hα-syn) for each time point.

Single-cell intracellular microinjections in SPNs

We carried out single-cell intracellular microinjections using previously published methods[63,67]. The 300 µm-thick striatal sections were mounted on nitrocellulose filter paper and immersed in 0.1 M PBS. Using DAPI as a staining guide, we identified the SPNs, impaled them with sharp micropipettes, and filled them with Alexa Fluor 568 hydrazide (Thermo Fisher Scientific, Waltham, MA) using a 1–20 nA direct current until the dye perfused the distal processes. Microinjections were performed on 10 neurons (5 per hemisphere); 1–2 sections were utilised per animal. Finally, the sections were mounted on glass slides with VectaShield mounting medium (Vector Laboratories, Burlingame, CA) and covered with 1.5 cover glasses (Corning).

High-resolution confocal microscopy and quantitative analysis of dendritic spine density and morphology

High-resolution dendritic spine imaging was performed using an upright Leica TCS SP8 confocal microscope (Leica Microsystems, Germany) with a resonance scanner and HyD detectors. We included 10 microinjected neurons per animal in the quantitative spine analysis. First, we obtained each neuron's low-resolution confocal z-stack image at 20x magnification. These images were used for an unbiased, systematic selection of segments for subsequent high-resolution imaging. Concentric rings were drawn around the soma 50 and 100 µm from the centre; then, we sampled the dendritic segments that crossed between the rings. Only dendritic segments parallel with the section were imaged while avoiding bifurcations, large fluctuations in the dendritic diameter and the first and last 10% of dendritic segments. Finally, we sampled between 10 and 20 dendritic segments per animal. Confocal z-stack images of each segment were taken at 63x magnification with a 63 × 1.4 numerical aperture oil-immersion objective (Leica Microsystems, Germany). Confocal z-stacks were acquired with an x, y resolution of 0.04 µm and a z step of 0.04 µm. We used Neurolucida 360 software (MicroBrightField Bioscience, Williston, VT) for semi-automatic 3D detection and analysis of the dendritic spines. Spines were first automatically detected, and an experimenter blinded to the condition then manually corrected obvious errors (e.g., a spine detected where there is no visible spine or a missed spine) to ensure that all spines had been appropriately identified. All spine measurements, including the head volume, were performed in 3D from the z-stacks obtained from each segment.

Our dendritic spines analysis focused on various morphometric parameters, including spine density, which quantifies the number of dendritic spines on a neuron's dendritic segment and provides insight into the density of synaptic connectivity. We also examined spine size—including measurements of spine head volume (μm^3), spine neck length (µm) and neck diameter (µm) —since changes in these dimensions can significantly influence synaptic strength and plasticity.

Spine head volume was calculated using Neurolucida 360 software, which defines the volume of the spine head as the total enclosed 3D space of the head, derived from the reconstruction generated during the automated detection process. The software calculates the volume by integrating the area of each cross-sectional plane along the z-axis (voxel-based measurement).

Dendritic spines exhibit diverse shapes, each with synaptic strength and stability implications. We used Neurolucida 360 to classify the spines according to morphometric type: thin, mushroom, stubby, and filopodia-like, drawing upon established criteria from previous studies[63,67]. A blinded experimenter detected and corrected errors after the preliminary, automated spine classification process. Spines with complex shapes (e.g., branched) were identified and categorised based on the presence of multiple spine heads attached to a single main spine neck[68]. Averages of dendritic segments analysed in each cell were obtained using a custom MATLAB script (Mathworks, Natick, MA). Afterwards, data were grouped by animal, group (EVV or hα-syn) for each time point. Importantly, a researcher blinded to the experimental conditions performed all imaging and quantification procedures.

Quantitative analysis of dendritic arborisation

Quantitative dendritic arborisation analysis included six microinjected neurons (3 from each hemisphere) per animal. Neurons were selected based on their well-defined, filled dendritic arbours, while those with a significant number of cut segments were excluded. Z-stacks of all neurons were acquired using a Zeiss Axioimager M1 microscope (Carl Zeiss AG, Germany) with 20x objective (Carl Zeiss AG, Germany) and a 1 µm step size. Images were analysed using the Simple Neurite Tracer (SNT) plugin in Fiji (NIH), where the experimenter created a 3D tracing of the neuron by drawing the dendrites that emerged from the soma. SNT recorded the x, y and z positions of each point the experimenter drew. The numerical values for each neuron's total dendritic length, number of branching points and terminal branches were extracted, along with a Sholl analysis to assess dendritic complexity. A branch point is defined as a location where a single dendritic segment bifurcates into two or more branches, reflecting the neuron's arborization and connectivity potential. A terminal branch refers to the endpoint of a dendrite that does not bifurcate further, indicating the neuron's maximum reach and potential synaptic connections. These parameters provide critical insights into the structural organization of neuronal dendrites and their capacity for connectivity and integration within neural circuits. Data were grouped by animal and group (EVV or hα-syn at 4 w p.i.; $n = 5$/group). A researcher blinded to the experimental conditions performed all imaging and quantification procedures.

Electron microscopy and quantitative ultrastructural analysis of dendritic spines

Animals from the hα-syn group at 72 h, 1 and 4 w p.i., and the EVV group as the control group ($n = 3$-4 per group and time point), were analysed. The rationale for time-point selection is provided in the experimental design paragraph. Brains were collected and processed for electron microscopy as previously described[5]. Striatal coronal sections previously processed for pre-embedding TH immunoperoxidase labeling, as described in a prior study[5], were used for the ultrastructural analysis of striatal dendritic spines. The sections were then washed twice in 0.1 M PB and they were post-fixed in 0.5% osmium tetroxide diluted in 0.1 M PB for 15 min. Following additional PB washes, the sections were dehydrated in ascending ethanol dilutions for 10 min each, and 1% uranyl acetate was added during the 70% ethanol step. The sections were then incubated in ethoxypropanol and embedded in epoxy resin (Durcupan™ ACM). Ultrathin sections from the superficial planes were obtained using an ultramicrotome, and these sections were contrasted with lead citrate and were examined with a transmission electron microscope (TEM; H-7650 microscope, Hitachi, Japan) equipped with an SC1000 Orius CCD camera (Gatan, Pleasanton, CA). Digital images were obtained randomly from the dorsal striatum of both hemispheres at a final magnification of 15,000x using Metamorph software (Molecular Devices, San Jose, CA). Images were collected systematically to avoid bias, and regions containing blood vessels, dense myelination, or astroglial swelling were excluded to ensure the focus was primarily on neurons and synapses. The X-Y plane image resolution was 3.4 nm/pixel, with an image size of 3284 × 2600 pixels. A total of 10 images were analysed using Fiji software (NIH) to determine the proportion of dendritic spines with SER visible on the head and the area of the spine head occupied by the SER. Manual tracking was performed by a researcher who was blinded to the experimental conditions. The calculated values were averaged across all animals for each group and time point.

Statistical analysis

All statistical analyses were performed using GraphPad Prism 8.0 software (GraphPad Software Inc., San Diego, CA). Data distribution for normality was assessed using the Kolmogorov-Smirnov test. The statistical differences between experimental groups and time points were determined by two-way ANOVA and Sidak or LSD multiple comparison tests. Statistical significance differences between the EVV group and multiple hα-syn time points were tested using the nonparametric Kruskal-Wallis and Dunn's multiple-comparison tests, and the t-test determined differences between the two experimental groups. The correlation analyses were performed using Pearson's parametric test. The results are expressed as mean ± SEM and statistically significant differences were considered at $P < 0.05$.

Data availability

The data supporting this study's findings are available from the corresponding author upon reasonable request.

Received: 30 September 2024; Accepted: 8 May 2025;
Published online: 03 June 2025

References

1. Kalia, L. V. & Lang, A. E. Parkinson's disease. *The Lancet*. https://doi.org/10.1016/S0140-6736(14)61393-3 (2015).
2. Spillantini, M. G. et al. α-synuclein in Lewy bodies. *Nature* https://doi.org/10.1038/42166 (1997).
3. Postuma, R. B. & Berg, D. Prodromal Parkinson's Disease: The Decade Past, the Decade to Come. *Movement Disorders.* https://doi.org/10.1002/mds.27670 (2019).
4. Blesa, J., Foffani, G., Dehay, B., Bezard, E. & Obeso, J. A. Motor and non-motor circuit disturbances in early Parkinson disease: which happens first? *Nat. Rev. Neurosci* https://doi.org/10.1038/s41583-021-00542-9 (2022).
5. Merino-Galán, L. et al. Striatal synaptic bioenergetic and autophagic decline in premotor experimental parkinsonism. *Brain* **145**, 2092–2107 (2022).
6. Calabresi, P. *et al*. Alpha-synuclein in Parkinson's disease and other synucleinopathies: from overt neurodegeneration back to early synaptic dysfunction. *Cell Death Dis* https://doi.org/10.1038/s41419-023-05672-9 (2023).
7. Kordower, J. H. et al. Disease duration and the integrity of the nigrostriatal system in Parkinson's disease. *Brain* **136**, 2419–2431 (2013).
8. Phan, J. A. et al. Early synaptic dysfunction induced by α-synuclein in a rat model of Parkinson's disease. *Sci. Rep.* **7**, 6363 (2017).
9. Decressac, M., Mattsson, B., Lundblad, M., Weikop, P. & Björklund, A. Progressive neurodegenerative and behavioural changes induced by AAV-mediated overexpression of α-synuclein in midbrain dopamine neurons. *Neurobiol. Dis*. **45**, 939–953 (2012).
10. Burke, D. A., Rotstein, H. G. & Alvarez, V. A. Striatal local circuitry: a new framework for lateral inhibition. *Neuron* https://doi.org/10.1016/j.neuron.2017.09.019 (2017).
11. Bridi, J. C. & Hirth, F. Mechanisms of α-Synuclein induced synaptopathy in parkinson's disease. *Front. Neurosci* https://doi.org/10.3389/fnins.2018.00080 (2018).
12. Ghiglieri, V., Calabrese, V. & Calabresi, P. Alpha-synuclein: From early synaptic dysfunction to neurodegeneration. *Front. Neurol.* https://doi.org/10.3389/fneur.2018.00295 (2018).
13. Imbriani, P., Schirinzi, T., Meringolo, M., Mercuri, N. B. & Pisani, A. Centrality of early synaptopathy in Parkinson's disease. *Front. Neurol.* https://doi.org/10.3389/fneur.2018.00103 (2018).
14. Tozzi, A. et al. Dopamine-dependent early synaptic and motor dysfunctions induced by a-synuclein in the nigrostriatal circuit. *Brain* **144**, 3477–3491 (2021).
15. Runge, K., Cardoso, C. & de Chevigny, A. Dendritic Spine Plasticity: Function and Mechanisms. *Front. Synaptic Neurosci.* https://doi.org/10.3389/fnsyn.2020.00036 (2020).
16. Calabresi, P., Picconi, B., Tozzi, A. & Di Filippo, M. Dopamine-mediated regulation of corticostriatal synaptic plasticity. *Trends Neurosci.* https://doi.org/10.1016/j.tins.2007.03.001 (2007).
17. Malinow, R. & Malenka, R. C. AMPA receptor trafficking and synaptic plasticity. *Ann. Rev. Neurosci* https://doi.org/10.1146/annurev.neuro.25.112701.142758 (2002).
18. Turrigiano, G. Homeostatic synaptic plasticity: Local and global mechanisms for stabilizing neuronal function. *Cold Spring Harb. Perspect. Biol*. **4**, a005736 (2012).
19. Turrigiano, G. G., Leslie, K. R., Desai, N. S., Rutherford, L. C. & Nelson, S. B. Activity-dependent scaling of quantal amplitude in neocortical neurons. *Nature* **391**, 892–896 (1998).
20. Blesa, J., Trigo-Damas, I., Quiroga-Varela, A. & Jackson-Lewis, V. R. Oxidative stress and Parkinson's disease. *Front. Neuroanat*. **9**, (2015). https://doi.org/10.3389/fnana.2015.00091
21. Minett, T. et al. Longitudinal diffusion tensor imaging changes in early Parkinson's disease: ICICLE-PD study. *J. Neurol.* **265**, 1528–1539 (2018).
22. Lisman, J. Glutamatergic synapses are structurally and biochemically complex because of multiple plasticity processes: Long-term potentiation, long-term depression, short-term potentiation and scaling. *Philos. Trans. R. Soc. B Biol. Sci.* **372**, 20160260 (2017).
23. Durante, V. et al. Alpha-synuclein targets GluN2A NMDA receptor subunit causing striatal synaptic dysfunction and visuospatial memory alteration. *Brain* **142**, 1365–1385 (2019).
24. Graves, S. M. & Surmeier, D. J. Delayed spine pruning of direct pathway spiny projection neurons in a mouse model of parkinson's disease. *Front. Cell. Neurosci*. **13**, (2019).
25. Picconi, B., Piccoli, G. & Calabresi, P. Synaptic dysfunction in Parkinson's disease. *Adv. Exp. Med. Biol.* **970**, 553–572 (2012).
26. Lieberman, O. J. et al. Dopamine triggers the maturation of striatal spiny projection neuron excitability during a critical period. *Neuron* **99**, 540–554 (2018).
27. Solis, O., Limón, D. I., Flores-Hernández, J. & Flores, G. Alterations in dendritic morphology of the prefrontal cortical and striatum neurons in the unilateral 6-OHDA-rat model of Parkinson's disease. *Synapse* **61**, (2007).
28. Villalba, R. M., Lee, H. & Smith, Y. Dopaminergic denervation and spine loss in the striatum of MPTP-treated monkeys. *Exp. Neurol*. **215**, (2009).
29. Garcia, B. G., Neely, M. D. & Deutch, A. Y. Cortical regulation of striatal medium spiny neuron dendritic remodeling in parkinsonism: Modulation of glutamate release reverses dopamine depletion-induced dendritic spine loss. *Cereb. Cortex* **20**, (2010).
30. Naskar, A. et al. Melatonin synergizes with low doses of L-DOPA to improve dendritic spine density in the mouse striatum in experimental Parkinsonism. *J. Pineal Res.* **55**, 304–312 (2013).
31. Villalba, R. M. & Smith, Y. Loss and remodeling of striatal dendritic spines in Parkinson's disease: from homeostasis to maladaptive plasticity? *J. Neural Trans.* https://doi.org/10.1007/s00702-017-1735-6 (2018).
32. Funamizu, Y. et al. Morphological dendritic spine changes of medium spiny neurons in the nucleus accumbens in 6-hydroxydopamine-lesioned rats treated with levodopa. *Neurosci. Res.* **121**, 49–53 (2017).
33. Gagnon, D. et al. Striatal Neurons Expressing D1 and D2 Receptors are Morphologically Distinct and Differently Affected by Dopamine Denervation in Mice. *Sci. Rep.* **7**, 41432 (2017).
34. McNeill, T. H., Brown, S. A., Rafols, J. A. & Shoulson, I. Atrophy of medium spiny I striatal dendrites in advanced Parkinson's disease. *Brain Res.* **455**, 148–152 (1988).
35. Stephens, B. et al. Evidence of a breakdown of corticostriatal connections in Parkinson's disease. *Neuroscience* **132**, 741–754 (2005).
36. Zaja-Milatovic, S. et al. Dendritic degeneration in neostriatal medium spiny neurons in Parkinson disease. *Neurology* **64**, 545–547 (2005).
37. Lundblad, M., Decressac, M., Mattsson, B. & Björklund, A. Impaired neurotransmission caused by overexpression of α-synuclein in nigral dopamine neurons. *Proc. Natl. Acad. Sci. USA*. **109**, 3213-3219 (2012).
38. Ingham, C. A., Hood, S. H. & Arbuthnott, G. W. Spine density on neostriatal neurones changes with 6-hydroxydopamine lesions and with age. *Brain Res*. **503**, (1989).
39. Suarez, L. M., Solis, O., Aguado, C., Lujan, R. & Moratalla, R. L-DOPA oppositely regulates synaptic strength and spine morphology in D1 and D2 striatal projection neurons in dyskinesia. *Cereb. Cortex* **26**, 4253–4264 (2016).
40. Villalba, R. M., Mathai, A. & Smith, Y. Morphological changes of glutamatergic synapses in animal models of Parkinson's disease. *Front. Neuroanatomy*. https://doi.org/10.3389/fnana.2015.00117 (2015).
41. Villalba, R. M. & Smith, Y. Striatal spine plasticity in Parkinson's disease. *Front. Neuroanat.* https://doi.org/10.3389/fnana.2010.00133 (2010).
42. Kashani, A., Betancur, C., Giros, B., Hirsch, E. & Mestikawy, S. El. Altered expression of vesicular glutamate transporters VGLUT1 and VGLUT2 in Parkinson disease. *Neurobiol. Aging* **28**, 568–578 (2007).

43. Zigmond, M. J., Abercrombie, E. D., Berger, T. W., Grace, A. A. & Stricker, E. M. Compensations after lesions of central dopaminergic neurons: some clinical and basic implications. *Trends Neurosci.* https://doi.org/10.1016/0166-2236(90)90112-N (1990).
44. Bezard, E., Gross, C. E. & Brotchie, J. M. Presymptomatic compensation in Parkinson's disease is not dopamine-mediated. *Trends Neurosci.* https://doi.org/10.1016/S0166-2236(03)00038-9 (2003).
45. Arkadir, D., Bergman, H. & Fahn, S. Redundant dopaminergic activity may enable compensatory axonal sprouting in Parkinson disease. *Neurology* **82**, 1093–1098 (2014).
46. Tønnesen, J., Katona, G., Rózsa, B. & Nägerl, U. V. Spine neck plasticity regulates compartmentalization of synapses. *Nat. Neurosci*. **17**, 678–685 (2014).
47. Grunditz, Å., Holbro, N., Tian, L., Zuo, Y. & Oertner, T. G. Spine neck plasticity controls postsynaptic calcium signals through electrical compartmentalization. *J. Neurosci*. **28**, 13457–13466 (2008).
48. Yuste, R. & Bonhoeffer, T. Genesis of dendritic spines: Insights from ultrastructural and imaging studies. *Nature Rev. Neurosci* https://doi.org/10.1038/nrn1300 (2004).
49. Holtmaat, A. & Svoboda, K. Experience-dependent structural synaptic plasticity in the mammalian brain. *Nature Rev. Neurosci* https://doi.org/10.1038/nrn2699 (2009).
50. Pchitskaya, E. & Bezprozvanny, I. Dendritic spines shape analysis—classification or clusterization? Perspective. *Front. Synaptic Neurosci* https://doi.org/10.3389/fnsyn.2020.00031 (2020).
51. Alberquilla, S., Gonzalez-Granillo, A., Martín, E. D. & Moratalla, R. Dopamine regulates spine density in striatal projection neurons in a concentration-dependent manner. *Neurobiol. Dis.* **134**, 104666 (2020).
52. Suarez, L. M., Solis, O., Sanz-Magro, A., Alberquilla, S. & Moratalla, R. Dopamine D1 Receptors Regulate Spines in Striatal Direct-Pathway and Indirect-Pathway Neurons. *Mov. Disord*. **35**, 1810–1821 (2020).
53. Tiroshi, L. & Goldberg, J. A. Population dynamics and entrainment of basal ganglia pacemakers are shaped by their dendritic arbors. *PLoS Comput. Biol.* **15**, e1006782 (2019).
54. Day, M., Wokosin, D., Plotkin, J. L., Tian, X. & Surmeier, D. J. Differential excitability and modulation of striatal medium spiny neuron dendrites. *J. Neurosci*. **28**, 11603-11614 (2008).
55. Surmeier, D. J., Ding, J., Day, M., Wang, Z. & Shen, W. D1 and D2 dopamine-receptor modulation of striatal glutamatergic signaling in striatal medium spiny neurons. *Trends Neurosci.* **30**, 228-235 (2007).
56. Korkotian, E. & Segal, M. Synaptopodin regulates release of calcium from stores in dendritic spines of cultured hippocampal neurons. *J. Physiol.* **589**, 5987–5995 (2011).
57. Chirillo, M. A., Waters, M. S., Lindsey, L. F., Bourne, J. N. & Harris, K. M. Local resources of polyribosomes and SER promote synapse enlargement and spine clustering after long-term potentiation in adult rat hippocampus. *Sci. Rep*. **9**, 3861 (2019).
58. Chinta, S. J. et al. Inducible alterations of glutathione levels in adult dopaminergic midbrain neurons result in nigrostriatal degeneration. *J. Neurosci.* **27**, 13997–14006 (2007).
59. Paget-Blanc, V. et al. A synaptomic analysis reveals dopamine hub synapses in the mouse striatum. *Nat. Commun.* **13**, 3102 (2022).
60. Kavalali, E. T. & Monteggia, L. M. Targeting homeostatic synaptic plasticity for treatment of mood disorders. *Neuron* **106**, 715–726 (2020).
61. Prieto, G. A. et al. Pharmacological rescue of long-term potentiation in Alzheimer diseased synapses. *J. Neurosci.* **37**, 1197–1212 (2017).
62. Belloso-Iguerategui, A. et al. Hippocampal synaptic failure is an early event in experimental parkinsonism with subtle cognitive deficit. *Brain* **146**, 4949–4963 (2023).
63. Dumitriu, D., Rodriguez, A. & Morrison, J. H. High-throughput, detailed, cell-specific neuroanatomy of dendritic spines using microinjection and confocal microscopy. *Nat. Protoc*. **6**, 1391–1411 (2011).
64. Paxinos, G. & Watson, C. The rat brain in stereotaxic coordinates. *London Acad. Press* 456 (2009).
65. Gonzalez-Reyes, L. E. et al. Sonic Hedgehog Maintains Cellular and Neurochemical Homeostasis in the Adult Nigrostriatal Circuit. *Neuron* **75**, 306–319 (2012).
66. West, M. J. Stereological methods for estimating the total number of neurons and synapses: Issues of precision and bias. *Trends Neurosci.* https://doi.org/10.1016/S0166-2236(98)01362-9 (1999).
67. Motley, S. E. et al. Selective loss of thin spines in area 7a of the primate intraparietal sulcus predicts age-related working memory impairment. *J. Neurosci.* **38**, 10467–10478 (2018).
68. Rochefort, N. L. & Konnerth, A. Dendritic spines: From structure to in vivo function. *EMBO Rep* https://doi.org/10.1038/embor.2012.102 (2012).

Acknowledgements

This study was funded by the Instituto de Salud Carlos III (ISCIII) through the projects PI14/00763 and PI19/01915, Co-funded by the European Regional Development fund 'A way to make Europe'. LM-G held a Predoctoral Research Fellowship from the University of the Basque Country (UPV/EHU) and two travel grants from the UPV/EHU and Boehringer Ingelheim, respectively, to perform consecutive research stays at Columbia University. AB-I held a Predoctoral Research Fellowship from the Government of the Basque Country. J.B held a Miguel Servet Program CP19/00200 from Instituto de Salud Carlos III. J.B and A.R-S are funded by Aligning Science Across Parkinson's [ASAP-020505] through the Michael J. Fox Foundation for Parkinson's Research (MJFF).The authors would like to thank the CIMA-Universidad Navarra, University of the Basque Country (UPV/EHU), Columbia University, and Boehringer Ingelheim for their support and use of their infrastructures.

Author contributions

L.M.G: Conceptualization, Data curation, Formal analysis, Investigation, Methodology, Visualization, Writing – original draft, Writing – review & editing. M.Z.: Data curation, Formal analysis, Investigation, Writing – review & editing. A.B.I.: Data curation, Formal analysis, Investigation, Methodology, Visualization, Writing – review & editing. M.A.M.: Data curation, Formal analysis, Writing – review & editing. B.G.: Data curation, Formal analysis, Writing – review & editing. A.R.S: Data curation, Writing – review & editing. J.B.: Methodology, Resources, Writing – review & editing. D.D.: Methodology, Resources, Writing – review & editing. A.Q.V: Conceptualization, Data curation, Formal analysis, Investigation, Methodology, Supervision, Writing – original draft, Writing – review & editing. M.C.R.O.: Conceptualization, Funding acquisition, Methodology, Supervision, Writing – review & editing.

Competing interests

M.C.R.O. received financial support for attending scientific meetings and lectures from Boston Scientific, Abbvie, Insightec, and Esteve. The rest of the authors report no competing interests or potential conflicts of interest.

Additional information

Supplementary information The online version contains supplementary material available at https://doi.org/10.1038/s41531-025-00994-1.

Correspondence and requests for materials should be addressed to María Cruz Rodríguez-Oroz.